On the state-of-the-art of CFD simulations for WECs within the open-source numerical framework of DualSPHysics

Alejandro J. Crespo, Bonaventura Tagliafierro, Iván Martínez-Estévez,
José M. Domínguez, Maite deCastro, Moncho Gómez-Gesteira, Corrado Altomare,
Moisés Brito, Francisco Bernardo, Rui Ferreira,
Salvatore Capasso, Giacomo Viccione,
Nicolas Quartier, Vasiliki Stratigaki, Peter Troch,
Irene Simonetti, Lorenzo Cappietti,
Malin Göteman, Jens Engström,
Daniel Clemente, Paulo Rosa-Santos, Francisco Taveira-Pinto,
Giorgio Bacelli, Ryan Coe,
Georgios Fourtakas, Benedict D. Rogers, Peter K. Stansby

Abstract—**To improve the design practice of marine renewable energy devices, it is imperative to adopt more robust methodologies. In light of this challenge, we present a systematic review that highlights the significance of utilising the Computational Fluid Dynamics (CFD)-based DualSPHysics software as a valuable support tool during the design stages of Wave Energy Converters (WECs). DualSPHysics, which is based on the Smoothed Particle Hydrodynamics (SPH) method, is a high-fidelity software tool that is inherently well-suited for addressing the diverse challenges associated with wave-WEC interactions. WECs are responsible for converting wave energy into usable forms, such as electricity, and a key component in this process is the Power Take-Off (PTO) system. To reliably replicate the important features involved in energy transformation, DualSPHysics leverages the coupling with the multiphysics library Project Chrono and the dynamic mooring model MoorDyn+. This augmented DualSPHysics framework enables the simulation of various types of WECs, encompassing different elements such as catenary connections, taut mooring lines, and both linear and non-linear PTO actuators. The objective of this study is twofold: to provide a comprehensive review of past applications utilising DualSPHysics and to showcase the versatility of this code in simulating a wide range of technologies within the marine renewable energy field. By demonstrating the capability of DualSPHysics in simulating diverse WEC technologies, we aim to contribute to the advancement of design practices and foster innovation in marine renewable energy.**

Index Terms—**WEC, OWSC, Point Absorber, Attenuator, Numerical Modelling, CFD, SPH, DualSPHysics**

Alejandro J. Crespo, Iván Martínez-Estévez, José M. Domínguez, Maite deCastro, Moncho Gómez-Gesteira - Universidade de Vigo, Spain (e-mail: alexbexe@uvigo.es, ivan.martinez.estevez@uvigo.es, jmdominguez@uvigo.es, mdecastro@uvigo.es, mggesteira@uvigo.es). Bonaventura Tagliafierro - Universidade de Vigo & UPC, Spain (e-mail: btagliafierro@gmail.com). Corrado Altomare - Universitat Politècnica de Catalunya, Spain (e-mail: corrado.altomare@upc.edu). Moisés Brito, Francisco Bernardo - Universidade Nova de Lisboa, Portugal (e-mail: moisesbrito@fct.unl.pt, fr.bernardo@campus.fct.unl.pt). Rui Ferreira - Instituto Superior Técnico, Portugal (e-mail: ruif@civil.ist.utl.pt). Salvatore Capasso, Giacomo Viccione - Università degli Studi di Salerno, Italy (e-mail: scapasso@unisa.it, gviccion@unisa.it). Nicolas Quartier, Vasiliki Stratigaki, Peter Troch - Ghent University, Belgium (e-mail: Nicolas.Quartier@ugent.be, Vicky.Stratigaki@ugent.be, Peter.Troch@ugent.be). Irene Simonetti, Lorenzo Cappietti - Università degli Studi di Firenze, Italy (e-mail: irene.simonetti@unifi.it, lorenzo.cappietti@unifi.it). Malin Göteman, Jens Engström - Uppsala University, Sweden (e-mail: malin.goteman@angstrom.uu.se, Jens.Engstrom@angstrom.uu.se). Daniel Clemente, Paulo Rosa-Santos, Francisco Taveira-Pinto - Universidade do Porto, Portugal (e-mail: up201009043@edu.fe.up.pt, pjrsantos@fe.up.pt, fpinto@fe.up.pt). Giorgio Bacelli, Ryan Coe - Sandia National Laboratories, USA (e-mail: gbacell@sandia.gov, rcoe@sandia.gov). Georgios Fourtakas, Benedict D. Rogers, Peter K. Stansby - The University of Manchester, UK (e-mail: georgios.fourtakas@manchester.ac.uk, benedict.rogers@manchester.ac.uk, p.k.stansby@manchester.ac.uk).

Digital Object Identifier:
https://doi.org/10.36688/ewtec-2023-145

I. Introduction

OCEAN energy, and in particular wave energy, has been recognised as widely available and abundant [1]. Concerning the very nature of wave energy, it has several advantages: waves are generated by wind patterns and storms over the oceans, making wave energy a consistent and technically unlimited resource. Its predictability in terms of the frequency, intensity, and direction [2] allows for better planning and integration [3]. Wave energy has higher density compared to wind or solar energy, implying that Wave Energy Converters (WECs) can generate more power using a smaller device or installation, leading to more efficient use of space [4]. Wave energy can complement other renewable energy technologies such as wind or solar power [5]. Integrating multiple renewable sources diversifies the energy mix, enhances reliability, and helps to meet electricity demand more effectively. Conversely, there are challenges to overcome, such as high upfront costs [6], survivability and maintenance, optimal PTO in operating conditions, performance under extreme loadings, efficiency in array layouts, potential impacts on marine ecosystems, and the need for suitable locations with favourable wave conditions. Nonetheless, ongoing research and technological advancements aim to address these challenges and unlock the full potential of wave energy as a sustainable energy solution.

WECs exhibit a wide range of shapes and operating principles, enabling their design to be tailored for various environmental conditions [7]. They are capable of harnessing wave energy through diverse physical transformation processes. However, further research is still needed to determine the optimal deployment practices for wave energy exploitation as a whole. Certain categories of WECs require mooring systems to ensure successful deployment and operation [8]. Mooring lines play a crucial role in maintaining the position of WEC devices, providing counteracting forces, and enabling efficient energy capture from the waves while ensuring stability and structural integrity. Another critical aspect lies in the Power Take-Off (PTO) mechanism [9], which involves the conversion of mechanical energy into more useful forms. The process mentioned above, considering the components' synergy, significantly influences the overall dynamics and interactions between the waves and the WEC structure.

The latest report from IRENA [10] shows that the net amount of marine power capacity has been stable at around 500 MW for the past 8 years. However,the outlook in the report [11] forecasts an installed capacity of 70 GW of ocean energy by 2030, with a relevant share taken up by wave energy [see also, 12]. Although the technology may be considered ready for immediate deployment [13], research has identified several weak spots in WEC technologies. The work of [14] highlighted that the service life of the WEC systems should be enhanced; especially, the service life of mooring lines and power cables used in these systems [15]. Guo and Ringwood [16] identified the need for a co-design approach to common fundamental issues, such as modelling, PTO and control design, survivability, and performance metrics. Another important piece of knowledge is provided by the report [17], in which it appears clear that the more devices are deployed, the cheaper the levelised cost of energy (LCoE) for wave energy gets.

Many uncertainties still persist regarding the response and survivability of WECs under adverse environmental conditions. These uncertainties have a negative impact on the LCoE, hindering the widespread commercial adoption of WEC technologies. In the pursuit of highly profitable locations [18], some WEC prototypes have been adapted to exploit areas with high power potential. Despite these challenges, one solution to mitigate the uncertainties surrounding WEC concepts and enhance their engineering is the utilisation of numerical modelling, since it can provide valuable insights and push forward the development of reliable WEC designs by leveraging solid data.

The first comprehensive review on numerical modelling strategies for investigating the hydrodynamic performance of WECs was proposed by Li and Yu [19], providing a methodical overview of the field. In terms of power production, practical approaches [20] and linear models are commonly utilised by the industry to achieve cost reductions in wave energy through optimisation [21]. However, while these approaches have contributed to minimising the total cost of energy (see above), they heavily rely on simplified design practices [22], requiring assumptions to account for viscous effects and wave superposition. It is important to note that these approaches have significant limitations, as highlighted by several authors who have cautioned against their use in analysing scenarios involving highly nonlinear interactions [23].

WEC simulations with Computational Fluid Dynamics (CFD)-based models represent one of the most useful tool for survivability analysis [24], which could be key to the economic success of WECs. Within this class of methods, mesh-based CFD methods are most common. However, in violent fluid-structure interactions, mesh deformation is a well-known challenge, often causing numerical instability and crashed simulations [24, 25]. Meshless CFD approaches have been suggested as feasible alternatives in these scenarios. Nevertheless, few applications can be found in the literature as reviewed in [26] and [25]. The Smoothed Particle Hydrodynamics (SPH) method [27, 28] is a particle-based (meshless) technique that has shown promise for a wide range of engineering applications [29], including offshore engineering [30]. An overview that surveys the SPH technique usability to simulate ocean energy devices is given in [31]. SPH has the advantage that wave-body interaction is easy to set up, initially with a wave basin filled with stationary particles and an imposed body displacing particles within its volume, being replaced by boundary particles. The fluid particles automatically organise themselves smoothly around the body. This is in contrast to mesh-based methods where body-fitted meshes are required, and this can be a time-consuming activity.

This paper compiles and orders the routine modelling and validation procedures available in the literature using the SPH-based solver DualSPHysics [32] applied to four different WEC types:

i) a moored point absorber (PA);
ii) an Oscillating Wave Surge Converter (OWSC);
iii) a floating OWSC (so-called FOSWEC);
iv) a multi-body attenuator (so-called Multi-float M4).

For each device listed above, we provide validation proof against physical model data for various components of the floater(s) and PTO related quantities, performed under specific sea conditions that aim to challenge their survivability. Within the scope of this research, we present the WEC response with respect to the degrees of freedom that really matter for each of the floaters due to hydrodynamic interactions (i.e., heave, surge, or pitch), along with quantities more intimately connected to the anchoring systems (e.g., line tension) or the mechanical apparatus (e.g., end-stop force). The quality of the results, the discussion built upon them, and the demonstrated solver exploitability to a wide range of WECs show that one software model can run all cases using the exact same methodology, which is of great value for the marine energy R&D community. Finally, we discuss future research objectives, which include the implementation of automation for open control systems and possible applications to subsets of WEC farm arrays (i.e., clusters) and other floating energy harnessing devices.

II. DualSPHysics code

A. SPH basis

DualSPHysics [32] implements the SPH Lagrangian meshless method, which is characterised by discretising a continuum with a set of particles (or computational nodes). The basis of the SPH method is represented mathematically by a convolution integral approximation of any function $F(\boldsymbol{r})$ as:

$$F(\boldsymbol{r}) = \int F(\boldsymbol{r}')W(\boldsymbol{r}-\boldsymbol{r}',h)\mathrm{d}\boldsymbol{r}' \tag{1}$$

Following this principle, the motion of each particle is obtained from the physical quantities of its neighbour particles, whose contribution is determined by a weighting function or kernel (W) with a region of influence defined by the smoothing length (h). The term $\boldsymbol{r}$ indicates the position of the point to compute the function, $\boldsymbol{r}'$ is the position of a neighbour computational point (or particle). Then, the function F is approximated by interpolating the particle contributions within the kernel support as:

$$F(\boldsymbol{r}_a) = \sum_b F(\boldsymbol{r}_b)W(\boldsymbol{r}_a-\boldsymbol{r}_b,h)\frac{m_b}{\rho_b} \tag{2}$$

where the subscripts a and b indicate the target particle and the neighbour particle, respectively, m is the mass, and ρ is the density. The kernel function $W(\boldsymbol{r},h)$ chosen in this work is the quintic Wendland [33]:

$$W(q) = \alpha_D\left(1-\frac{q}{2}\right)^4(2q+1), \text{ with } 0\le q\le 2 \tag{3}$$

where $q = r/h$ is the non-dimensional distance between particles, r the distance between particles a and b, and being α_D=21/16πh^3 in three dimensions.

In DualSPHysics, the smoothing length h is defined as a function of the initial inter-particle distance, dp, used to create the initial condition. In the simulations of this work, we use h=1.7dp, so that the kernel support, using the quintic function, will be 2h=3.4dp.

B. Governing equations

The motion of the particles is governed by the discrete form of the Navier-Stokes equations in fluid dynamics. Thus, the momentum equation can be written as:

$$\frac{\mathrm{d}\boldsymbol{v}_a}{\mathrm{d}t} = -\sum_b m_b\left(\frac{p_a+p_b}{\rho_a\rho_b}+\Pi_{ab}\right)\nabla_a W_{ab}+\boldsymbol{g}, \tag{4}$$

$$\Pi_{ab} = \begin{cases}\left(\frac{-\alpha\overline{c_s}_{ab}}{\overline{\rho_{ab}}}\right)\left(\frac{h\boldsymbol{v}_{ab}\cdot\boldsymbol{r}_{ab}}{r_{ab}^2+0.01^2}\right) & \boldsymbol{v}_{ab}\cdot\boldsymbol{r}_{ab}<0\\ 0 & \boldsymbol{v}_{ab}\cdot\boldsymbol{r}_{ab}>0\end{cases} \tag{5}$$

being $(\cdot)_{ab}=(\cdot)_a-(\cdot)_b$, t is the time, $\boldsymbol{v}$ is the velocity, p is the pressure, $\boldsymbol{g}$ is the gravity acceleration, and c_s is the numerical speed of sound. An artificial viscosity term (Π_{ab}) is included in the continuity equation, as proposed by Monaghan [34].

Moreover, the continuity equation is expressed as:

$$\frac{\mathrm{d}\rho_a}{\mathrm{d}t} = \rho_a\sum_b\frac{m_b}{\rho_b}\boldsymbol{v}_{ab}\cdot\nabla_a W_{ab}+D_a, \tag{6}$$

$$D_a = 2\delta h\, c_s\sum_b(\rho_{ba}^T-\rho_{ab}^H)\frac{\boldsymbol{r}_{ab}\cdot\nabla_a W_{ab}}{r_{ab}^2}\frac{m_b}{\rho_b} \tag{7}$$

being D_a the density diffusion term added to the continuity equation, following the formulation presented in Fourtakas et al. [35]. The term δ is the coefficient that controls the diffusive term (0.10), and superscripts T and H are the total and hydrostatic components of the density, respectively. Then, the hydrostatic pressure is computed as $\rho_{ab}^H=\rho_0 g z_{ab}$, where z_{ab} is the difference of the position in z between particles a and b.

DualSPHysics implements a weakly compressible SPH formulation, for which an equation of state is employed to compute the fluid pressure (p) from the density (ρ) as:

$$p = \frac{c_s^2\rho_0}{\gamma_p}\left[\left(\frac{\rho}{\rho_0}\right)^{\gamma_p}-1\right] \tag{8}$$

where ρ_0 is the reference density of the fluid and γ_p=7 is the polytropic constant.

C. Boundary conditions and rigid body dynamics

The modified Dynamic Boundary Conditions (mDBC) method proposed by English et al. [36] is implemented in DualSPHysics. This approach is an improvement of the original DBC method previously presented in Crespo et al. [37] that allows for more accurate results at lower resolutions. The arrangement of the boundary particles using mDBC follows the basis of DBC. However, in this novel approach, a boundary interface is defined at a certain distance from the innermost layer of boundary particles, generally at $dp/2$ for simple geometries. Then, normal vectors are created from the boundary particles to the boundary interface, pointing to the fluid. Those vectors are used to mirror ghost nodes into the fluid domain and boundary particles obtain the fluid properties computed by a corrected SPH approximation at the ghost node. More details of this novel implementation are presented in [36].

D. Coupling with a multiphysics engine

The multiphysics engine Project Chrono [38] has been coupled with the DualSPHysics code and presented by Martínez-Estévez et al. [39]. In this coupling technique, the SPH method solves the fluid-solid interaction while the multiphysics engine solves the solid-solid interaction by using the Discrete Element Method (DEM) introducing complementarity conditions (the so-called DEM-C) [40]. Following [38], the dynamics of the multibody systems composed by rigid bodies is computed as a linear transformation of the generalised positions and velocities. Each body can experience external forces (for which the reaction lies outside the given system) and constraint forces. In this work, the forces exerted by the fluid due to the fluid-solid interaction are intended as external forces, whereas forces induced by the mechanical constraints among the internal. The effect of PTOs belong to this latter. The formulation used in order to solve linear mechanical systems associated to the PTOs are related to the following formulae:

$$F_{PTO} = \ k_c\,(d-l) + c_c v_z \tag{9}$$

$$F_{PTO} = \ k_r\theta + \ c_r\dot{\theta} \tag{10}$$

Equation (9) refers to the mechanical constraint applied by a translational spring-damper-actuator (TSDA), where d is the distance between the origins of the attached rigid bodies, l is the equilibrium length of the spring, v_z is the relative velocity, and k_c and c_c are the linear stiffness and damping coefficient, respectively. On the other hand, (10) refers to the revolute joint, where $\boldsymbol{\theta}$ is the relative angle of rotation, $\dot{\boldsymbol{\theta}}$ is the angular velocity, and k_r and c_r are the rotational stiffness and damping coefficients, respectively. More complex PTO actuators, nonlinear mechanical constraints and contacts such as joints and sliders, friction and restitution coefficients, restitution forces, and user imposed forces and trajectories with arbitrary degrees of freedom can be included in the code.

E. Coupling with a mooring solver

DualSPHysics has been coupled with the mooring solver MoorDyn+ [41] to simulate moored fluid-driven objects. The mooring solver employs a lumped-mass approach to address the problem. The lumped-mass technique involves partitioning the entire unstretched length of the line (L_0) into N equally-long segments, resulting in a total of N+1 nodes. The properties of each segment are inherited from the overall geometry of the line, which is defined by several parameters. The segment length is given by $l = L_0/N$. The volume-equivalent area (A) is calculated as $A = \pi d^2/4$, where d represents the volume-equivalent diameter. The density of the line material is denoted by ρ. The net mass of each segment, represented by m_i, is determined by $Al(\rho - \rho_w)$, where ρ_w is the density of the surrounding water. The elasticity modulus is denoted by E, and the internal damping coefficient is represented as C_{int}. By utilising this lumped-mass approach, the solver accurately models the behaviour of the mooring line based on its geometric and material properties.

III. Validation of WECs using DualSPHysics

The work of [42] was one of the first to use SPH to look at the behaviour of a floating WEC point absorber in focused waves. Since then, the number of published research papers focused on the SPH modelling of WECs has been growing, suggesting that the capability of this meshless methodology to study the efficiency, and above all, the survivability of the devices is growing as well. The present research aims to prove the capability of DualSPHysics of studying different technologies with the same solver including mooring connections and different PTO systems. In particular, four devices are simulated with the latest v5.2 version (https://dual.sphysics.org). The simulated devices are: i) a moored point absorber (UWEC); ii) an Oscillating Wave Surge Converter (OWSC); iii) a floating OWSC (FOSWEC); and iv) the multi-body attenuator M4. Figure 1 shows the four models and layouts, and relevant features of the WECs are provided in Table I.

Table I
Relevant features of the four WEC designs.

Name	Technology	Mooring	PTO type
UWEC	Point absorber	Taut line	Linear
OWSC	OWSC	None	Rotational
FOSWEC	OWSC	Taut lines	Rotational
Multi-float M4	Attenuator	Catenary line	Rotational

In the following subsections, the four simulated devices are described and validated against physical test data. Two different resolutions (dp) are used to obtain the numerical results proposed in this research. Note that the wave-WEC interaction should be solved using a spatial resolution that does not only consider the wave heights but also the characteristic dimensions of the devices. In any case, in this work we follow a common criterion for the four simulated WECs, so the approach suggested in [43] requiring wave heights represented by at least 10 dp is used. The first resolution aims to use 10-15 particles per maximum wave height (indicated as ”medium”), whereas the second envisions resolution up to 25 particles (”high” resolution). At the end of each section, we include some information on the numerical studies conducted in some recent publications and discuss the benefits of using DualSPHysics to complement the design phases of those devices.

A. Uppsala Point Absorber

The Uppsala WEC belongs is a point-absorber, as it consists of a floating buoy, for which the dominant size facing waves is much smaller than the wavelength. The wave-activated motion of the buoy is converted into electricity by means of a PTO system. The UWEC point absorber combines a floating buoy (with various shapes) and a linear magnet generator (PTO) connected via a line. The generator is attached on a ballasted platform and located at the seabed. A taut mooring line transmits the rectified motion of the buoy to the translator. In the early 2000s, some archetype models of this device were installed in pilot wave power plants off the Sweden coast [44]. Subsequently, Göteman et al. [45] investigated the UWEC performance under embedded focused and irregular waves to mimic extreme wave conditions in the test facility at Plymouth University (UK). The testing was carried out at a 1:20 scale and has previously been used for validation of mesh-based CFD codes [46–49].

The UWEC has been validated using DualSPHysics, as presented in [50], comparing with the experimental setup presented in [45]. The UWEC configuration comprised a cylindrical buoy of height 0.11 m, diameter of 0.17 m and an initial draft of 0.03 m, and connected to the PTO (with end-stoppers) mechanical systems

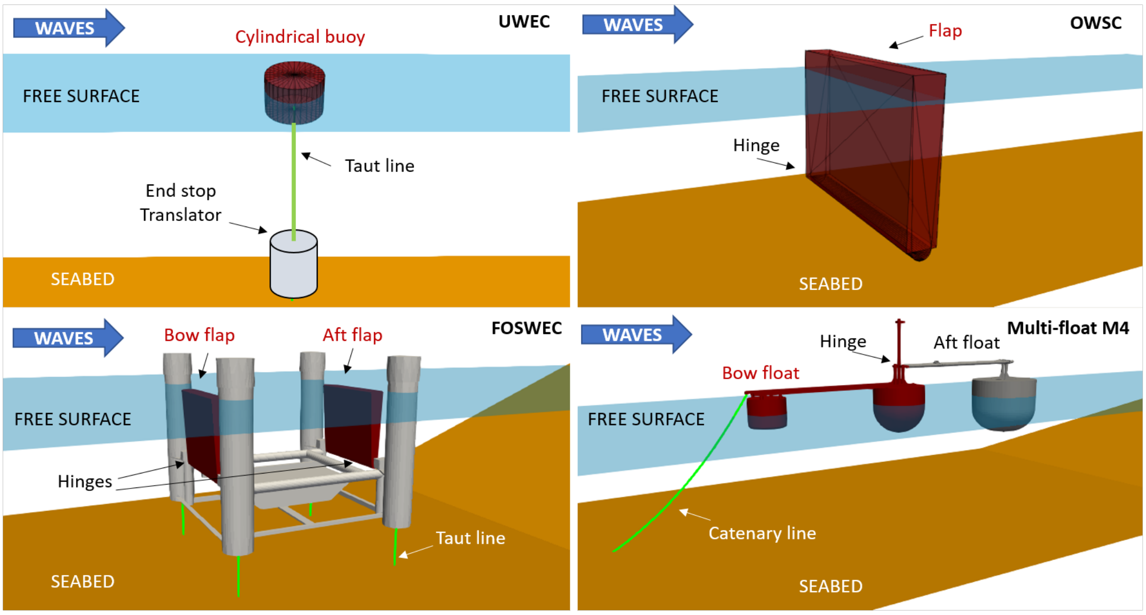

Figure 1. Schematic representation of the WECs to be simulated here with the same version of DualSPHysics.

(coupling with Project Chrono) and a mooring line (coupling with MoorDyn+). The selected wave conditions (embedded focused train) regards the description of an extreme event characterised by maximum wave height of H=0.36 m and wave period T=2.39 s, travelling in 2.50-meter water depth. Two PTO configurations were taken into account, in which the harvesting system was not operational (internal damping 2.79 Ns/m), and when the harvesting function was activated (including extra friction resistance of 6.75 N). Here, we present the outcome for the first case alone. An instant of the simulation with DualSPHysics v5.2 is shown in Figure 2, where the particle colouring represents the horizontal velocity of the fluid.

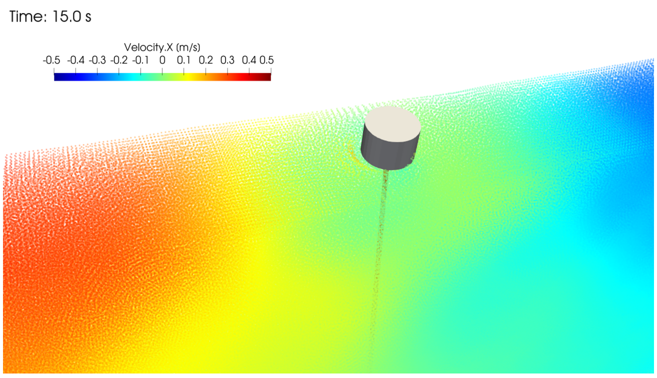

Figure 2. Simulation snapshot of the UWEC interacting with waves (medium resolution).

Figure 3 compares numerical outputs with experimental data for the tested wave configuration defined above. Note that the wave flume, PTO numerical arrangement, and the mooring setup are given in [50]. The first panel in Figure 3 compares the free-surface elevation (η) sampled at the focusing location for undisturbed wave propagation. For both numerical resolutions, the model agreement is good, implying that the medium resolution is sufficient to capture the surface dynamics. In the remaining panels, the response of the buoy (surge and heave) and the mooring line (tension T) are reported. The surge panel reports a 30% underestimation of the sinking motion of the buoy, and in the opposite way, the heave motion provides excellent matching with the reference solution, capturing also small perturbations that are induced by the snap loads into the line, shown in the last panel. Overall, the high resolution (25 particles per wave height) does not resolve into critical changes in the hydrodynamic response of the system compared to the medium one (17 particles per wave height). Regardless, the framework provided by the high resolution allows capturing with accuracy the peak response of the mooring line.

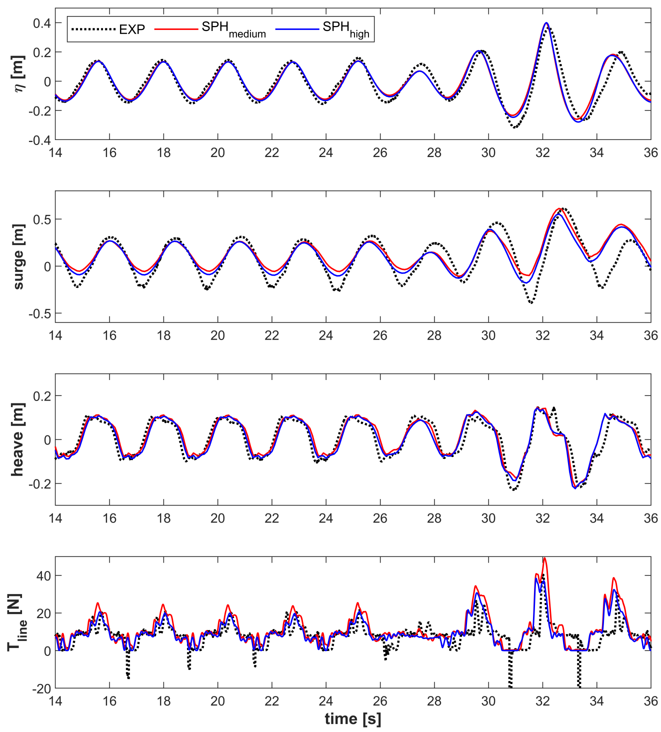

Figure 3. Comparison between experimental and numerical time series of free-surface elevation, surge and heave motions of the UWEC and tension in the taut line, where subscripts *medium* and *high* denote SPH resolutions of dp=0.021 m and dp=0.014 m, respectively.

In Tagliafierro et al. [50], DualSPHysics was subsequently employed to perform a survivability study, using irregular sea state representation to model high-return period wave conditions for marine structures, comprising the modelling of 500 waves. The investigation suggests that efficient management of the PTO internal parameters could enhance the capability of the device, for short- and long-term conditions, thus supporting more robust and resilient design procedure. Furthermore, follow-up research proposed in [51], where the same validated device was used in DualSPHysics, has explored the sensitivity of focused wave configurations to its critical design parameters.

B. Oscillating Wave Surge Converter

Oscillating Wave Surge Converters (OWSCs) are designed to harness wave energy nearshore, primarily in shallow waters, by capturing wave energy through an oscillatory pitch motion. OWSCs take advantage of favourable wave mechanics in shallow waters [52, 53], offering benefits such as reduced upfront and maintenance costs. Noteworthy research on the lower hinged OWSC concept is documented in [54], which provides experimental data for validating numerical models [55, 56]. Brito et al. [55] presents a series of laboratory tests conducted to validate the dynamics of an OWSC under water waves. These tests took place in a horizontal wave flume at the Instituto de Mecánica de los Fluidos e Ingeniería Ambiental (IMFIA) in Uruguay. The flap of the OWSC consists of PVC tubes joined by a stainless steel frame, and a bearing, and it is hinged width-wise at a height of 0.10 m above the flume bed. The dimensions of the flap are as follows: height of 0.84 m, width of 1.31 m, and thickness of 0.17 m, with a mass of 72.3 kg. The PTO system comprises a hydraulic cylinder and a closed hydraulic circuit connected to both the flap and the flume bed.

The validation presented in Brito et al. [57] was conducted for four regular wave conditions with a still water depth of 0.825 m. The wave parameters, including wave height and period, were represented by plane progressive waves as follows: R1=(0.15 m, 2.0 s), R2=(0.25 m, 2.0 s), R3=(0.20 m, 3.0 s), and R4=(0.25 m, 3.5 s). A particle spatial convergence analysis was performed in a 2-D setting to assess the choice of dp on the accuracy of predicted free-surface elevations. The PTO system was also included in the modelling to account for the effects of friction and pressure forces within the hydraulic system, which serves as the energy outlet for the system. The friction torque on the revolute joint between the flap and hinge bearings was modelled using an equivalent torque generated by a linear force that adheres to Coulomb damping behaviour (Chrono coupling [39]). The R2 test condition was simulated again using the latest version of DualSPHysics (v5.2) and a 3-D computational domain (see Figure 4). To generate the regular waves, a piston-type wavemaker was positioned upstream of the computational domain.

Figure 5 presents the validation of the OWSC response under regular waves. In the first panel, the wave profile (η) generated and propagated into the

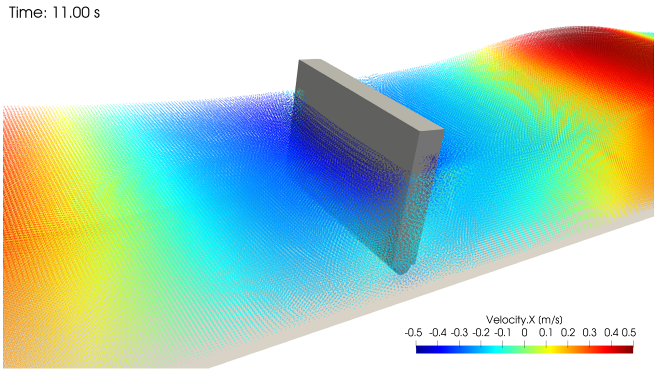

Figure 4. Simulation snapshot of the OWSC device (medium resolution).

numerical model at the virtual location of the device is shown. The two solid lines represent the fluid resolution of the SPH model, demonstrating minor peak and trough underestimation. The following three panels compare the angular position (θ), the angular velocity (ω), and the angular acceleration (α) of the flap with the experimental reference motion. The numerical model can accurately predict the dynamic behaviour of the flap under cyclic excitation, displaying satisfactory accuracy. With an SPH medium resolution (12 particles per wave height), good agreement between the numerical and experimental time series is achieved. Increasing the SPH resolution further (25 particles per wave height) does not significantly enhance the accuracy.

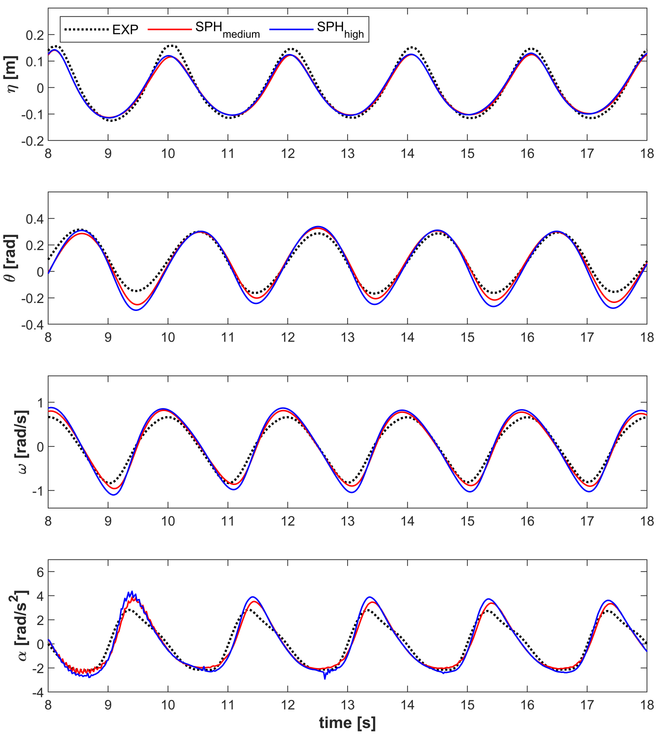

Figure 5. Comparison between experimental and numerical time series of free-surface elevation, rotation of the flap, angular velocity and angular acceleration of the OWSC, where subscripts *medium* and *high* denote SPH resolutions of dp=0.02 m and dp=0.01 m, respectively.

The influence of the PTO system on the hydrodynamics of OWSC was numerically analysed through the change of the PTO setup [57]. The effects of the mechanical constraints, damping coefficients, and flap inertia on the hydrodynamics of the OWSC were also studied. It was found that these factors significantly influenced the response amplitude and phase. The friction coefficient had a more significant effect than the pressure coefficient on the Capture Width Ratio (CWR). Additionally, varying the flap mass, centre of mass, height, and thickness also affected the CWR, with a higher dependence on flap height. The study highlights the potential of using SPH and multiphysics solvers for OWSC design and testing in virtual laboratories.

C. Floating Oscillating Surge Wave Energy Converter

As mentioned in the introduction, one approach to reduce the LCoE of WECs involves combining simple WECs with other marine structures. This can be observed in cases where offshore wind floating platforms co-host point absorbers [58–60], or when coastal marine defensive structures incorporate OWSCs [61, 62]. Similarly, the Floating Oscillating Surge Wave Energy Converter (FOSWEC) is an innovative device introduced in [63], with a slightly improved configuration proposed in [64, 65]. The FOSWEC consists of a dual-flap device with a submerged central platform serving as the host for the two flaps. The flaps are hinged to pivot around shafts mounted to the hull and are controlled by independent motors, simulating the energy extraction process (i.e., the PTO). The buoyancy of the device is maintained by four surface-piercing foam-filled vertical PVC structures, while the hull is anchored to the tank bottom by four mooring taut vertical lines. Experimental tests were conducted in the Directional Wave Basin of the O.H. Hinsdale Wave Research Laboratory (HWRL) at the Oregon State University.

The FOSWEC model has been validated in [66] using specific data obtained from Coe et al. [64]. The experimental investigation aimed to conduct system identification tests and investigate closed-loop control systems, which typically require a large dataset obtained from relatively linear conditions [67]. The FOSWEC model is configured to enable accurate multiphysics simulations where the dynamics of multiple bodies become crucial. In the experimental setup, the platform, which provides a buoyancy force of 540 N, is placed in the flume, and the two flaps (bow and aft) are connected using revolute joints capable of applying restoring and dissipative forces. The assembly is further connected to the seabed through four tension legs, with each line experiencing an equilibrium tension of 135 N. The reference dimension for this setup is the mean flap width, which is 0.05 m. The wave conditions analysed in this study are taken from Test ID 194 [64], defined by H=0.136 m, T=1.56 s, and d=1.36 m (water depth). The overall assembly of the numerical FOSWEC is visualised in Figure 6, under the action of regular waves.

Figure 7 illustrates the validation of the FOSWEC numerical model. In the first panel, a comparison is made between the numerical and experimental results, considering the wave profile over a time window of five fully developed wave cycles. The model exhibits a high level of fidelity, accurately capturing the shape of the waves. The second and third panels depict the pitch angles for the bow and aft flaps, respectively, as computed by DualSPHysics for two different resolutions (13 and 27 particles per wave height) and compared to the experimental data. The model predictions closely align with the reference data, and the higher resolution leads to more precise estimations for both flap responses. Notably, a significant improvement in the quality of the solution can be observed in the fourth panel, which represents the line tension. It is evident that increasing the SPH resolution results in a more consistent response of the mooring line, indicating a more accurate representation of its behaviour. When compared to the paper [66], better agreement has been found regarding the tension in the mooring lines, most likely related to more accurate buoyant forces.

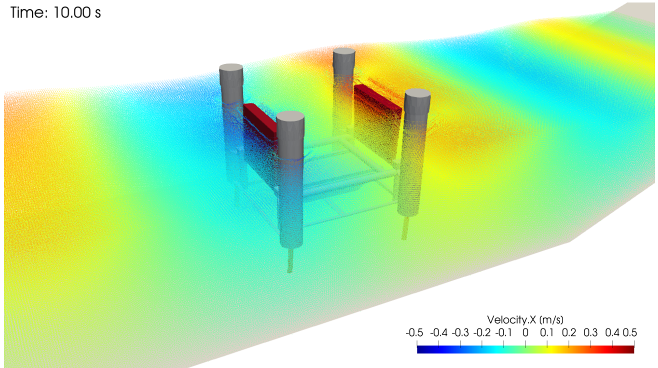

Figure 6. Simulation snapshot of the FOSWEC under the action of regular waves (medium resolution).

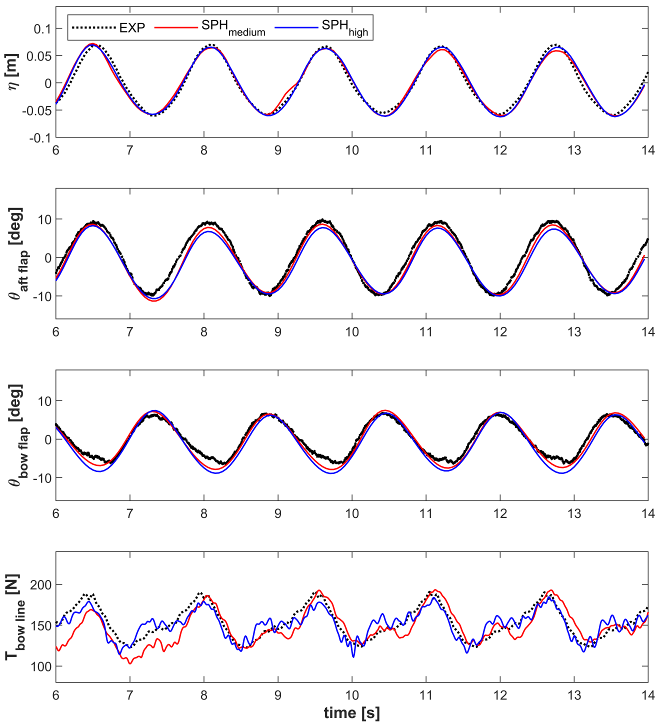

Figure 7. Comparison between experimental and numerical time series of free-surface elevation, rotations of the bow and aft flaps and tension in one of the bow lines of the FOSWEC, where subscripts *medium* and *high* denote SPH resolutions of dp=0.01 m and dp=0.005 m, respectively.

In the reference work [66], a comprehensive validation was conducted, encompassing a broader spectrum of scenarios. The study included dry setup simulations, specifically focusing on the flap decay test. Moreover, the motion of the platform was validated by comparing it with surge motion and pitch angle measurements. Simulating the FOSWEC remains a significant challenge due to the complex interactions between multiple bodies and the utilisation of active and passive control techniques during experimental tests. However, in the case of the present SPH solver, the hydrodynamic interaction between the fluid and the flaps posed a particularly difficult challenge. This was attributed to the small thickness of the flaps, which made the application of the mDBC method challenging.

D. Multi-float M4

The multi-float M4 is a WEC concept that comprises several floats with multi-mode forcing. The cylindrical floats have different diameters and drafts with hemispherical bases to minimise losses due to drag. The diameters of the floats and their drafts increase from bow to aft (wave direction) to facilitate the alignment with the wave direction due to wave-induced mean forces [68]. The physical tests to design the multi-float M4 took place in the COAST (Coastal, Ocean and sediment Transport) laboratory of Plymouth University. The M4 model configuration tested here is the early design with three in-line floaters with the smallest float at the bow and largest at the stern. The bow-float and mid-float are rigidly connected, the stern float is connected by a rod to a hinge on a vertical column on the mid-float allowing angular rotation at the hinge. This relative angular displacement was measured by an angular encoder. More details of the experimental tests can be found in [69].

The work [70] utilised DualSPHysics to simulate extreme conditions on the M4 device under focused waves. The extreme event was generated with a specific focus position. The referenced study [70] modelled and validated the version of the M4 device with three floats, employing three different wave sets. The wave trains consisted of focused wave groups with peak spectral periods (T_p) of 1.00, 1.10, and 1.20 s, respectively. The waves had a peak enhancement factor (γ) of 3.3, linear crest amplitude (A_c) of 0.08 m, and water depth of 0.60 m. The mid float of the M4 device was positioned at the focal point (x_f). To accurately represent the device behaviour, Project Chrono was utilised to model the hinge constraint between the mid and stern floats. Additionally, the MoorDyn+ library was used to attach a mooring line directly from the basin floor to the bow float with a length of 1.00 m. However, it is important to note that in the experimental tests, a mooring line with a mooring buoy was employed. The primary objective of the experimental tests was to capture the maximum converter response to the extreme wave without mechanical damping. In this work, the focused wave with T_p=1.10 s has been reproduced (Figure 8), and the simulation incorporates mDBC applied to the floats and utilises the density diffusion term proposed in [35].

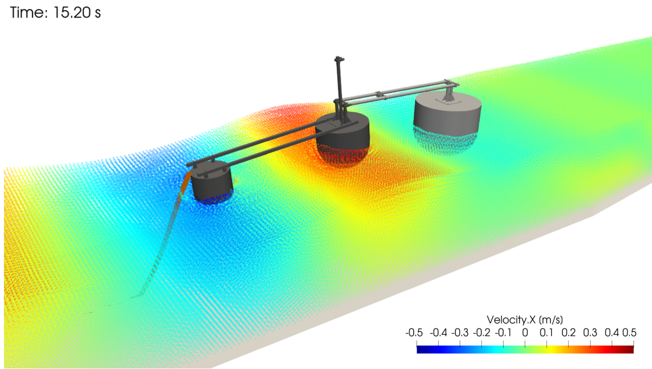

Figure 8. A snapshot of the simulation of Multi-float M4 under the action of focused waves (medium resolution).

Figure 9 presents the validation results for the M4 validation using a defined focused wave group. The top panel compares the numerical time series of water-surface elevation with the measured data at the focusing position for validation. In the bottom panel, the relative angular displacement (θ) between the aft and bow floats is compared. An accurate free-surface elevation is achieved for this setup, which proves to be more accurate than the initial one. As such, satisfactory agreement is achieved between the experimental angular response magnitude and the numerical simulation results for different particle resolutions. However, a slight phase shift is observed in the simulation during the last few seconds. This deviation may be attributed to the difficulty of precisely maintaining the device around the focusing position in the simulation, as the numerical approach uses only a catenary line instead of the mooring buoy employed in the experiments. The discrepancy in angular response phase could stem from this difference in numerical methodology. Nonetheless, the results obtained using version 5.2 demonstrate consistently good matching and appear to be more accur-

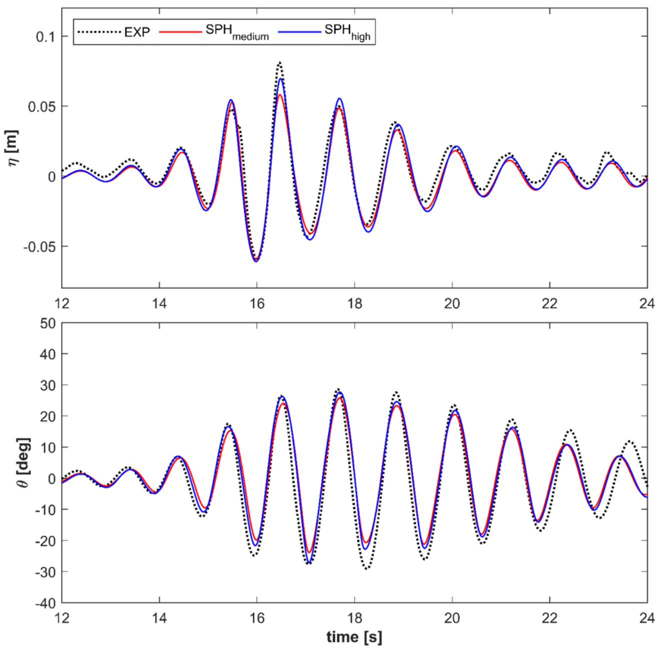

Figure 9. Comparison between experimental and numerical time series of free-surface elevation at the focused position and angular response of the Multi-float M4, where subscripts *medium* and *high* denote SPH resolutions of dp=0.02 m and dp=0.01 m, respectively.

ate than those presented in [70]. This improvement can potentially be achieved thanks to the utilisation of new boundary conditions (mDBC) applied to the complex float geometries, as well as the latest implementations on density diffusion terms. Additionally, a more precise wave generation technique may also contribute to the enhanced accuracy.

However, it is crucial to acknowledge that [70] marked the pioneering instance of combining an SPH model with mechanical constraints (resolved by Project Chrono) and a mooring line model (resolved by MoorDyn+) to simulate such complex interactions. With advancements leading to enhanced accuracy in applying mDBC to such geometries, the time is now ripe for analysing the device behaviour upon activating the PTO mechanism.

IV. Conclusions and future work

This paper provides a review of the application of DualSPHysics v5.2 in simulating four well-established WEC concepts. These concepts encompass a wide range of features and scenarios, thereby providing insights into simulating other novel WEC devices. For each device, we present a brief overview of its working principles and revised the results obtained from re-simulations using the latest unified code version. In our analyses, we observed mild to significant improvements compared to the original validation results presented in the reference papers. These improvements can be attributed to the utilisation of the novel scheme for boundary conditions (mDBC) and the implementation of an advanced new smoothing density filter. Notably, the previous validations, such as that of M4, have been enhanced as a result.

By conducting these simulations and showcasing the improvements achieved with the updated DualSPHysics framework, our study aims to make a valuable contribution to the expanding field of WEC simulation. Moreover, our research has led to the initiation of two additional investigations in related areas. The first investigation focuses on a Wave Energy Hyperbaric Converter (WEHC) [71], which aims to explore new possibilities in wave energy conversion. The second one revolves around the development of E-Motions, a complex Power Take-Off (PTO) system that harnesses wave-induced roll oscillations on multipurpose offshore floating platforms [72]. These ongoing studies build upon the knowledge gained from our research and hold promise for further advancements in the field.

The research and development undertaken by the working group is poised to yield more comprehensive and tangible outcomes for the marine renewable energy sector. A significant milestone in this endeavour is the release of version 5.2 of DualSPHysics, which represents a consolidation of the collective efforts (as developers and users) of this research community, holding great potential for addressing previously unchallenged issues.

Acknowledgement

The authors of this work gratefully acknowledge the support provided by the WECANet COST Action (CA17105 - A pan-European Network for Marine Renewable Energy). This support has facilitated short-term scientific missions for numerous researchers from various institutions involved in this study. This work was supported by the project SURVIWEC PID2020-113245RB-I00 financed by MCIN/AEI/10.13039/501100011033 and by the project ED431C 2021/44 "Programa de Consolidación e Estructuración de Unidades de Investigación Competitivas" financed by Xunta de Galicia, Consellería de Cultura, Educación e Universidade, Spain.

References

[1] N. Khan et al. "Review of ocean tidal, wave and thermal energy technologies". In: *Renewable and Sustainable Energy Reviews* 72 (2017), pp. 590–604.

[2] B. Reguero et al. "A global wave power resource and its seasonal, interannual and long-term variability". In: *Applied Energy* 148 (2015), pp. 366–380.

[3] D. Clemente et al. "On the potential synergies and applications of wave energy converters: A review". In: *Renewable and Sustainable Energy Reviews* 135 (2021), p. 110162.

[4] E. Dallavalle et al. "Improved methodology for the optimal mixing of renewable energy sources and application to a multi-use offshore platform". In: *Renewable Energy* 210 (2023), pp. 575–590.

[5] M. W. Ayub et al. "A Review of Power Co-Generation Technologies from Hybrid Offshore Wind and Wave Energy". In: *Energies* 16.1 (2023).

[6] C. Guo et al. "A Review of the Levelized Cost of Wave Energy Based on a Techno-Economic Model". In: *Energies* 16.5 (2023).

[7] A. F. de O. Falcão. "Wave energy utilization: A review of the technologies". In: *Renewable and Sustainable Energy Reviews* 14.3 (2010), pp. 899–918.

[8] S. Xu et al. "Review of mooring design for floating wave energy converters". In: *Renewable and Sustainable Energy Reviews* 111 (2019), pp. 595–621.

[9] R. Ahamed et al. "Advancements of wave energy converters based on power take off (PTO) systems: A review". In: *Ocean Engineering* 204 (2020).

[10] International Renewable Energy Agency. *Renewable Capacity Statistics 2023*. Tech. rep. Abu Dhabi: International Renewable Energy Agency, 2023.

[11] IRENA. *World Energy Transitions Outlook 2022: 1.5°C Pathway*. Abu Dhabi: International Renewable Energy Agency, 2022.

[12] T. Kober et al. "Global energy perspectives to 2060 – WEC's World Energy Scenarios 2019". In: *Energy Strategy Reviews* 31 (2020).

[13] D. Magagna et al. "Ocean energy development in Europe: Current status and future perspectives". In: *International Journal of Marine Energy* 11 (2015), pp. 84–104.

[14] A. Uihlein et al. "Wave and tidal current energy – A review of the current state of research beyond technology". In: *Renewable and Sustainable Energy Reviews* 58 (2016), pp. 1070–1081.

[15] M. Melikoglu. "Current status and future of ocean energy sources: A global review". In: *Ocean Engineering* 148 (2018), pp. 563–573.

[16] B. Guo et al. "A review of wave energy technology from a research and commercial perspective". In: *IET Renewable Power Generation* 15.14 (2021), pp. 3065–3090.

[17] IRENA and OEE. *Scaling up investments in ocean energy technologies*. International Renewable Energy Agency, Abu Dhabi. 2023.

[18] L. Rusu et al. "The performance of some state-of-the-art wave energy converters in locations with the worldwide highest wave power". In: *Renewable and Sustainable Energy Reviews* 75 (2017), pp. 1348–1362.

[19] Y. Li et al. "A synthesis of numerical methods for modeling wave energy converter-point absorbers". In: *Renewable and Sustainable Energy Reviews* 16.6 (2012), pp. 4352–4364.

[20] R. G. Coe et al. "A practical approach to wave energy modeling and control". In: *Renewable and Sustainable Energy Reviews* 142 (2021), p. 110791.

[21] A. Garcia-Teruel et al. "Hull geometry optimisation of wave energy converters: On the choice of the objective functions and the optimisation formulation". In: *Applied Energy* 298 (2021), p. 117153.

[22] J. Davidson et al. “Linear parametric hydrodynamic models for ocean wave energy converters identified from numerical wave tank experiments”. In: *Ocean Engineering* 103 (2015), pp. 31–39.

[23] J. van Rij et al. “A Wave Energy Converter Design Load Case Study”. In: *Journal of Marine Science and Engineering* 7.8 (2019).

[24] E. Ransley et al. “Survivability of wave energy converters using CFD”. In: *Renewable Energy* 109 (2017), pp. 235–247.

[25] J. Davidson et al. “Efficient Nonlinear Hydrodynamic Models for Wave Energy Converter Design—A Scoping Study”. In: *Journal of Marine Science and Engineering* 8.1 (2020).

[26] C. Windt et al. “High-fidelity numerical modelling of ocean wave energy systems: A review of computational fluid dynamics-based numerical wave tanks”. In: *Renewable and Sustainable Energy Reviews* 93 (2018), pp. 610–630.

[27] J. J. Monaghan et al. “Gravity currents descending a ramp in a stratified tank”. In: *Journal of Fluid Mechanics* 379 (1999), pp. 39–69.

[28] M. Gomez-Gesteira et al. “SPHysics - development of a free-surface fluid solver - Part 1: Theory and formulations”. In: *Computers & Geosciences* 48 (2012), pp. 289–299.

[29] A. Amicarelli et al. “SPHERA v.9.0.0: A Computational Fluid Dynamics research code, based on the Smoothed Particle Hydrodynamics mesh-less method”. In: *Computer Physics Communications* 250 (2020).

[30] H. Gotoh et al. “On the state-of-the-art of particle methods for coastal and ocean engineering”. In: *Coastal Engineering Journal* 60.1 (2018), pp. 79–103.

[31] H.-G. Lyu et al. “A Review of SPH Techniques for Hydrodynamic Simulations of Ocean Energy Devices”. In: *Energies* 15.2 (2022).

[32] J. M. Domínguez et al. “DualSPHysics: from fluid dynamics to multiphysics problems”. In: *Computational Particle Mechanics* 9.5 (2022), pp. 867–895.

[33] H. Wendland. “Piecewise polynomial, positive definite and compactly supported radial basis functions of minimal degree”. In: *Advances in Computational Mathematics* 4.1 (1995), pp. 389–396.

[34] J. Monaghan. “Smoothed Particle Hydrodynamics”. In: *Annual Review of Astronomy and Astrophysics* 30.1 (1992), pp. 543–574.

[35] G. Fourtakas et al. “Local uniform stencil (LUST) boundary condition for arbitrary 3-D boundaries in parallel smoothed particle hydrodynamics (SPH) models”. In: *Computers & Fluids* 190 (2019), pp. 346–361.

[36] A. English et al. “Modified dynamic boundary conditions (mDBC) for general-purpose smoothed particle hydrodynamics (SPH): application to tank sloshing, dam break and fish pass problems”. In: *Comp. Part. Mech.* 9.5 (2022), pp. 911–925.

[37] A. Crespo et al. “Boundary conditions generated by dynamic particles in SPH methods”. In: *Computers, Materials and Continua* 5.3 (2007), pp. 173–184.

[38] A. Tasora et al. “Chrono: An Open Source Multi-physics Dynamics Engine”. In: 2016, pp. 19–49.

[39] I. Martínez-Estévez et al. “Coupling of an SPH-based solver with a multiphysics library”. In: *Computer Physics Communications* 283 (2023), p. 108581.

[40] M. Anitescu et al. “An iterative approach for cone complementarity problems for nonsmooth dynamics”. In: *Comput. Optim. Appl.* (2010).

[41] J. Domínguez et al. “SPH simulation of floating structures with moorings”. In: *Coastal Engineering* 153 (2019), p. 103560.

[42] P. Omidvar et al. “SPH for 3D floating bodies using variable mass particle distribution”. In: *International Journal for Numerical Methods in Fluids* 72.4 (2013), pp. 427–452.

[43] C. Altomare et al. “Long-crested wave generation and absorption for SPH-based DualSPHysics model”. In: *Coastal Engineering* 127 (2017), pp. 37–54.

[44] R. Waters et al. “Experimental results from sea trials of an offshore wave energy system”. In: *Applied Physics Letters* 90.3 (2007), p. 034105.

[45] M. Göteman et al. “Wave Loads on a Point-Absorbing Wave Energy Device in Extreme Waves”. In: vol. All Days. International Ocean and Polar Engineering Conference. 2015.

[46] J. Engström et al. “Buoy geometry and its influence on survivability for a point absorbing wave energy converter: Scale experiment and CFD simulations”. In: *School of Engineering, Computing and Mathematics* (2017), p. 4.

[47] L. Sjökvist et al. “Numerical models for the motion and forces of point-absorbing wave energy converters in extreme waves”. In: *Ocean Engineering* 145 (2017), pp. 1–14.

[48] E. Katsidoniotaki et al. “Response of Point-Absorbing Wave Energy Conversion System in 50-Years Return Period Extreme Focused Waves”. In: *Journal of Marine Science and Engineering* 9.3 (2021).

[49] E. Katsidoniotaki et al. “Numerical modeling of extreme wave interaction with point-absorber using OpenFOAM”. In: *Ocean Engineering* 245 (2022), p. 110268.

[50] B. Tagliafierro et al. “A numerical study of a taut-moored point-absorber wave energy converter with a linear power take-off system under extreme wave conditions”. In: *Applied Energy* 311 (2022), p. 118629.

[51] B. Tagliafierro et al. “Investigation into embedded focused wave group suitability for the assessment of extreme hydrodynamics loads on point-absorber WECs”. In: *Trends in Renewable Energies Offshore*. 2023, pp. 421–430.

[52] M. Folley et al. “The effect of water depth on the performance of a small surging wave energy converter”. In: *Ocean Engineering* 34.8 (2007), pp. 1265–1274.

[53] T. Whittaker et al. “Nearshore oscillating wave surge converters and the development of Oyster”. In: *Philosophical Transactions of the Royal Society A: Mathematical, Physical and Engineering Sciences* 370.1959 (2012), pp. 345–364.

[54] Y. Wei et al. “Wave interaction with an oscillating wave surge converter, Part I: Viscous effects”. In: *Ocean Engineering* 104 (2015), pp. 185–203.

[55] M. Brito et al. “Experimental investigation on the power capture of an oscillating wave surge converter in unidirectional waves”. In: *Renewable Energy* 151 (2020), pp. 975–992.

[56] C. Zhang et al. “SPHinXsys: An open-source multi-physics and multi-resolution library based on smoothed particle hydrodynamics”. In: *Computer Physics Communications* 267 (2021), p. 108066.

[57] M. Brito et al. “A numerical tool for modelling oscillating wave surge converter with nonlinear mechanical constraints”. In: *Renewable Energy* 146 (2020), pp. 2024–2043.

[58] M. J. Muliawan et al. “Extreme responses of a combined spar-type floating wind turbine and floating wave energy converter (STC) system with survival modes”. In: *Ocean Engineering* 65 (2013), pp. 71–82.

[59] Y. Si et al. “The influence of power-take-off control on the dynamic response and power output of combined semi-submersible floating wind turbine and point-absorber wave energy converters”. In: *Ocean Engineering* 227 (2021), p. 108835.

[60] K. Sun et al. “Experimental investigation of semi-submersible platform combined with point-absorber array”. In: *Energy Conversion and Management* 245 (2021), p. 114623.

[61] X. Zhao et al. “Analytical investigation on the hydrodynamic performance of a multi-pontoon breakwater-WEC system”. In: *Ocean Engineering* 220 (2021), p. 108394.

[62] S. Saeidtehrani et al. “Multipurpose breakwater: Hydrodynamic analysis of flap-type wave energy converter array integrated to a breakwater”. In: *Ocean Engineering* 235 (2021), p. 109426.

[63] K. Ruehl et al. “Experimental and numerical comparisons of a dual-flap floating oscillating surge wave energy converter in regular waves”. In: *Ocean Engineering* 196 (2020), p. 106575.

[64] R. G. Coe et al. “FOSWEC dynamics and controls test report”. In: (2020).

[65] D. D. Forbush et al. “Design and testing of a free floating dual flap wave energy converter”. In: *Energy* 240 (2022).

[66] B. Tagliafierro et al. “Numerical Modeling of Moored Floating Platforms for Wave Energy Converters Using DualSPHysics”. In: vol. 5-A. American Society of Mechanical Engineers (ASME), 2022.

[67] D. Ogden et al. “Review of WEC-Sim Development and Applications”. In: *International Marine Energy Journal* 5.3 (2022), pp. 293–303.

[68] P. Stansby et al. “Capture width of the three-float multi-mode multi-resonance broadband wave energy line absorber M4 from laboratory studies with irregular waves of different spectral shape and directional spread”. In: *Journal of Ocean Engineering and Marine Energy* 1.3 (2015), pp. 287–298.

[69] H. Santo et al. “Extreme motion and response statistics for survival of the three-float wave energy converter M4 in intermediate water depth”. In: *Journal of Fluid Mechanics* 813 (2017), pp. 175–204.

[70] E. Carpintero Moreno et al. “Response of the multi-float WEC M4 in focussed waves using SPH”. In: 2020.

[71] M. Brito et al. “Numerical Model of Constrained Wave Energy Hyperbaric Converter under Full-Scale Sea Wave Conditions”. In: *Journal of Marine Science and Engineering* 10.10 (2022).

[72] D. Clemente et al. “Numerical developments on the E-Motions wave energy converter: Hull design, power take-off tuning and mooring system configuration”. In: *Ocean Engineering* 280 (2023).